

Investigations in High Temperature Single Crystal X-ray Crystallography^a

A. M. Shaikh

Abstract | Single crystal analysis has the advantage of giving more detailed and significant information in several areas related to structure than the analysis of polycrystalline materials. One important investigation would be the X-ray determination of atomic vibration amplitudes over a range of temperatures up to melting point in simple structures. This would throw considerable light on the phenomenon of melting, besides providing a reliable check on the validity of the lattice dynamical models used to predict the phonon characteristics of solids. Accurate experimental data needed for such investigations call for suitable high temperature devices, which can be conveniently attached to commercially available single crystal cameras and diffractometers. Investigations in the field of high temperature single crystal X-ray diffraction were done at Physics Department, Indian Institute of Science, Bangalore during 1970–1980. Varieties of heater attachments based on resistance heating, gas flame and hot air flow technique were developed for use with commercially available single crystal X-ray cameras and diffractometers. These include heater attachments for Weissenberg camera (1000 °C–3000 °C), Hilger & Watts linear diffractometer (1000 °C), Charles Super Co. precession camera (1000 °C), a complete high temperature Weissenberg camera for single crystal data collection up to 400 °C in vacuum or inert gas atmosphere and up to 900 °C in air, a high temperature attachment for Enraf-Nonius CAD-4 Kappa axis diffractometer (500 °C). Accurate single crystal X-ray diffraction data on NaCl, and KCl were collected on linear diffractometer from room temperature to melting point for study of thermal vibration of atoms. High temperature data with CAD-4 diffractometer was collected for study of phase transition in ferroelectric sodium metavanadate and dicalcium lead propionate, semiconductor to metal transition in Ti_2O_3 and Jahn Teller induced phase transition in $CsCuCl_3$. The present article describes the salient features of the various high temperature techniques developed and high temperature crystallographic studies made.

^aThis article is dedicated to the fond memory of late Prof. M.A. Viswamitra who inspired me with importance of instrumentation in scientific research.

*Solid State Physics
Division, Bhabha Atomic
Research Centre, Mumbai
400085, India
shaikham@barc.gov.in*

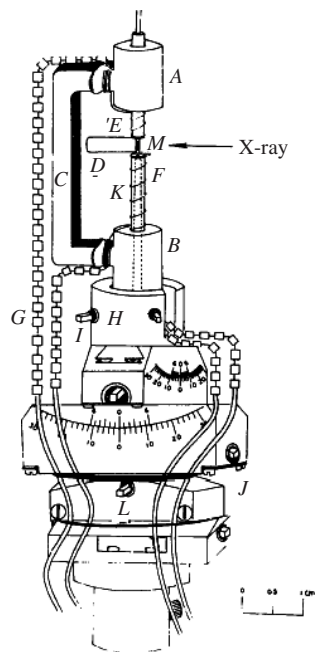
Keywords: X-ray
Crystallography, Single
Crystal cameras, Four circle
diffractometer, Crystal heater,
Phase transition

1. Introduction

The beginning of high temperature X-ray crystallography could be traced to as early as

1914 when Bragg [1] demonstrated, at elevated temperatures, the diminution of X-ray intensities from NaCl also the change in the reflecting

Figure 1: Schematic representation of the furnace mounted on a standard goniometer head. A and B Quartz tubes connected by bracket C. E and F Silica tubes on which is wound the heater wire D. G Glass bead insulated platinum lead wire. H Brass mount for the furnace, with side screws I. J Goniometer. K Thermocouple probe inside F. M Experimental crystal at the middle of the X-ray gap.



positions due to the expansion of the lattice. Since then high temperature techniques have been used for the study of materials for wide range of problems such as phase transformation, thermal expansion, stress effects at elevated temperatures, condensation reactions, crystal structure analysis and thermal vibrations. Excellent reviews of high temperature diffraction techniques available since then have appeared [2–5]. Although a wide variety of furnaces has been devised for the study of powder specimens, relatively little has been published on high temperature devices suitable for single crystal X-ray analysis. Single crystal analysis, however, has the advantage of giving more detailed and significant information in several areas related to structure than the analysis of polycrystalline materials. One important investigation would be the x-ray determination of atomic vibration amplitudes over a range of temperatures up to melting point in simple structures. This would throw considerable light on the phenomenon of melting, besides providing a reliable check on the validity of the lattice dynamical models used to predict the phonon characteristics of solids. Accurate experimental data needed for such investigations call for suitable high temperature devices, which can be conveniently attached to commercially available single crystal cameras and diffractometers.

Investigations in the field of high temperature single crystal X-ray diffraction was initiated by Late Prof. M.A. Viswamitra in 1968 at Physics Department, Indian Institute of Science, Bangalore. Varieties of heater attachments based on resistance heating, gas flame and hot air flow technique were

Figure 2: View of the furnace on S.35 Unicam Weissenberg camera in the vertical mounting.

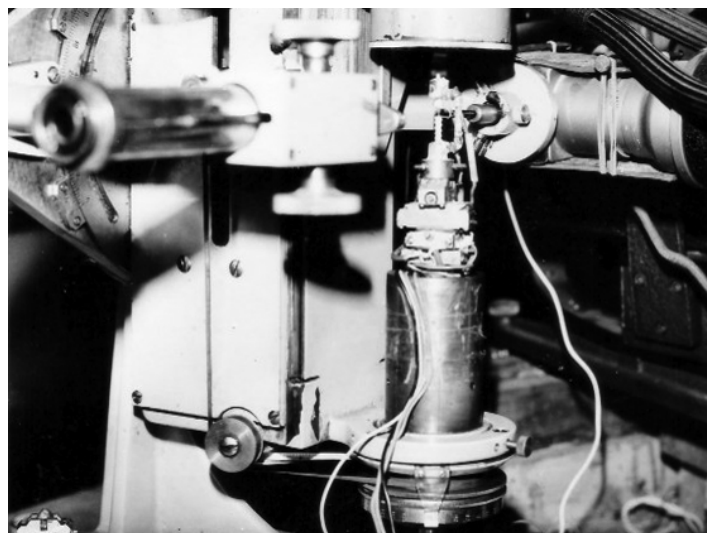


Figure 3: Oscillation photograph of NaCl at 25 °C and 560 °C with exposure of one hour (left) and zero level Weissenberg photograph of NaCl taken at 25 °C, 505 °C and 752 °C. Exposure 2 hrs. each (right side).

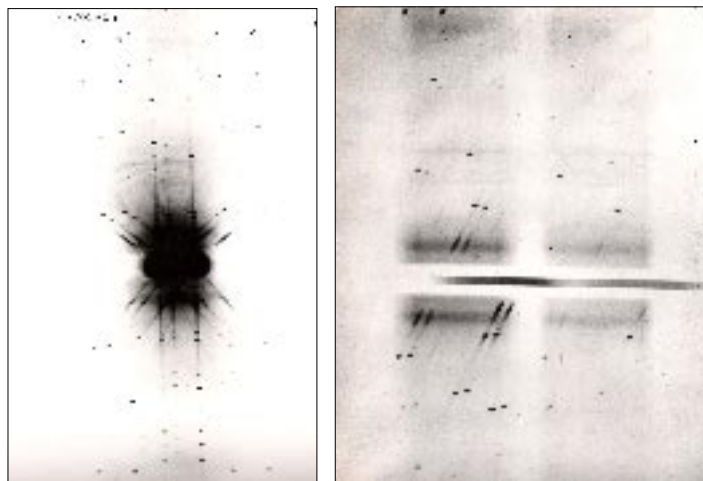
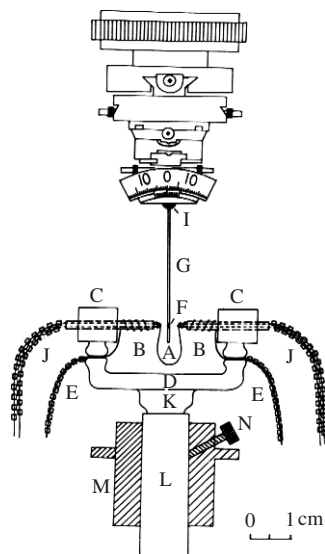


Figure 4: Schematic representation of furnace assembly. A, platinum-wire heating element; B, twin-bore silica tubes; C, quartz tube in which B is mounted; D, quartz bracket; E, platinum lead wires; F, experimental crystal mounted inside the silica capillary G; H, goniometer head; I, Autostick ceramic cement; J, Pt-Pt/13 Rh thermocouples; K, quartz stem inside brass holder L; M, brass collar; N, height adjusting screw.



developed for use with commercially available single crystal X-ray cameras and diffractometers. These include heater attachments for Weissenberg camera (1000 °C–3000 °C), Hilger & Watts linear diffractometer (1000 °C), Charles Super Co. precession camera (1000 °C), a complete high temperature Weissenberg camera for single crystal data collection up to 400 °C in vacuum or inert

gas atmosphere and up to 900 °C in air, a high temperature attachment for Enraf-Nonius CAD-4 Kappa axis diffractometer (500 °C). Accurate single crystal X-ray diffraction data on NaCl, and KCl were collected on linear diffractometer from room temperature to melting point for study of thermal vibration of atoms. High temperature data with CAD-4 diffractometer was collected for

Figure 5: Furnace mounted in the linear diffractometer.

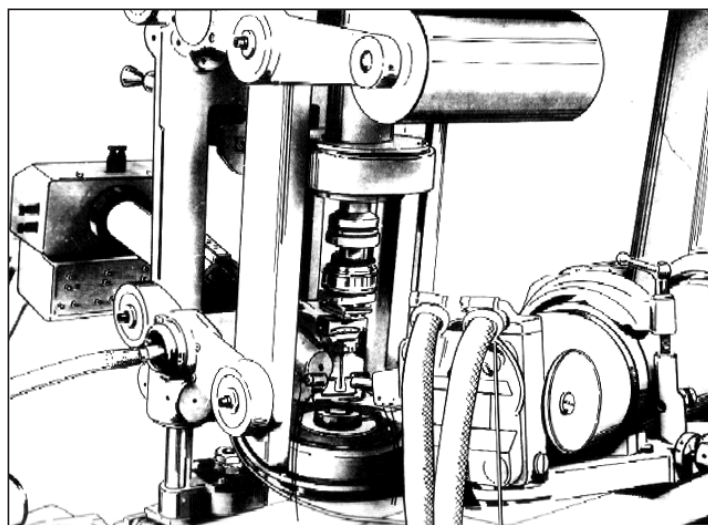
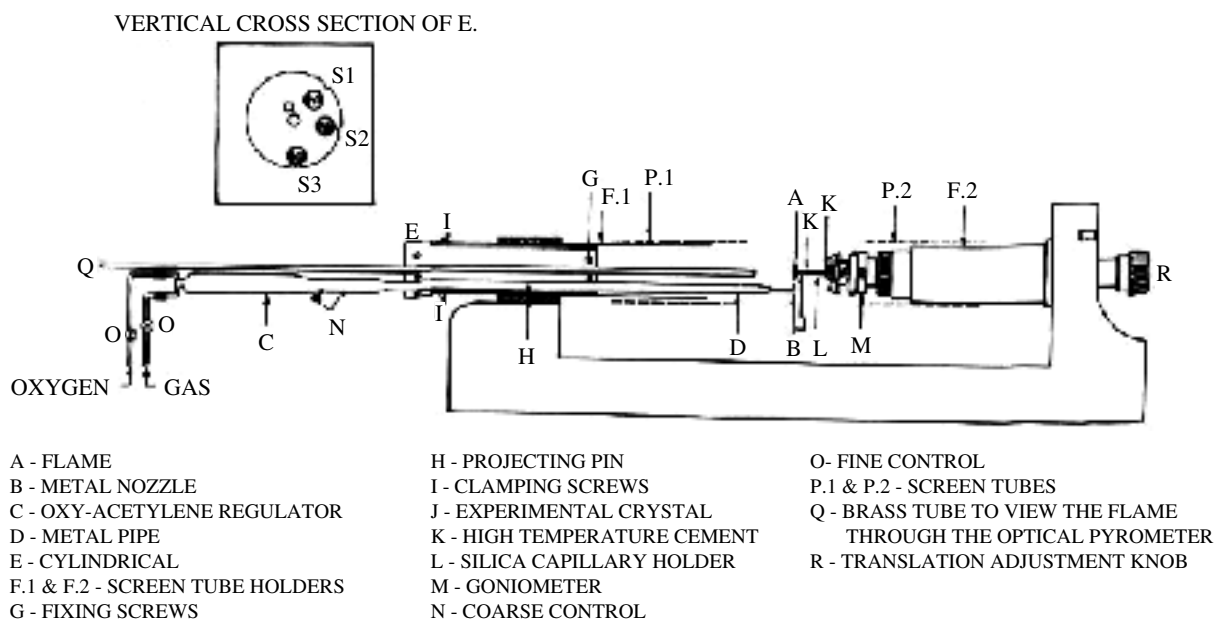


Figure 6: Schematic Diagram of Flame Technique with Nonius Weissenberg camera.



study of phase transition in ferroelectric sodium metavanadate and dicalcium lead propionate, semiconductor to metal transition in Ti_2O_3 and Jahn Teller induced phase transition in $CsCuCl_3$. The present article describes the salient features of the various high temperature techniques developed and high temperature crystallographic studies made. In addition author's post I.I.Sc. work on high temperature X-ray study of minerals is also given.

2. Development of high temperature techniques for single crystal cameras and diffractometers

2.1. A Miniature furnace suitable for X-ray Weissenberg photography up to $1000^\circ C$ [6].

A miniature furnace suitable for routine single crystal data collection up to $1000^\circ C$ was designed and used in conjunction with a Unicam S35 Weissenberg camera. The sample is heated primarily

by radiation from a surrounding, current-heated split platinum coil. It has many desirable features like easy replacement of heater coil and experimental crystal and elimination of any water-cooling requirement. The details are shown in Fig. 1. The present furnace, as such, can also be mounted inside a horizontal Weissenberg camera and has the additional possibility of use up to 1500 °C after replacing the silica tubes E and F by suitable alumina tubes. In both these cases, however, the film-cassette will have to be water-cooled.

2.2. A simple miniature furnace for routine collection of single crystal x-ray data up to 1000 °C on the Hilger and Watts linear diffractometer [7].

A miniature furnace suitable for routine collection of x-ray data up to 1000 °C from single crystals on

the Hilger and Watts linear diffractometer, without restricting the normally allowed region of reciprocal space on the diffractometer, is described. The crystal is heated primarily by radiation from a surrounding current-heated, stationary platinum coil wound on a silica bracket. The coil is split at its middle to provide a 4 mm gap for crystal mounting and x-irradiation. The crystal, mounted on a standard goniometer head, can be rotated and centred freely, as in the room temperature case. There is no need for any radiation shields or water-cooling arrangement. Investigations up to 1500 T are possible with slight modifications of the furnace. The furnace has been extensively used to collect the intensity data from several crystals of NaCl up to the melting point and of KCl up to 765 °C, the results of have been published elsewhere.

Figure 7: Hinged split cassette for taking high temperature X-ray photographs on Nonius camera using flame technique.

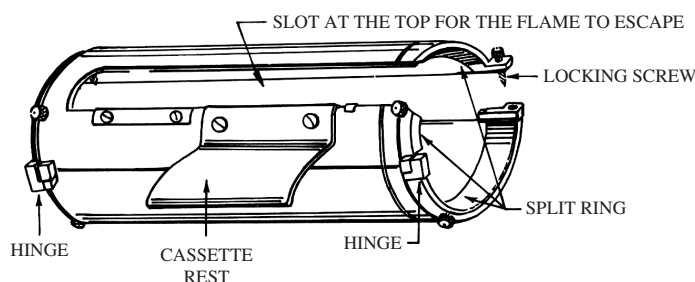


Figure 8: The flame heating device on the Nonius Weissenberg camera.

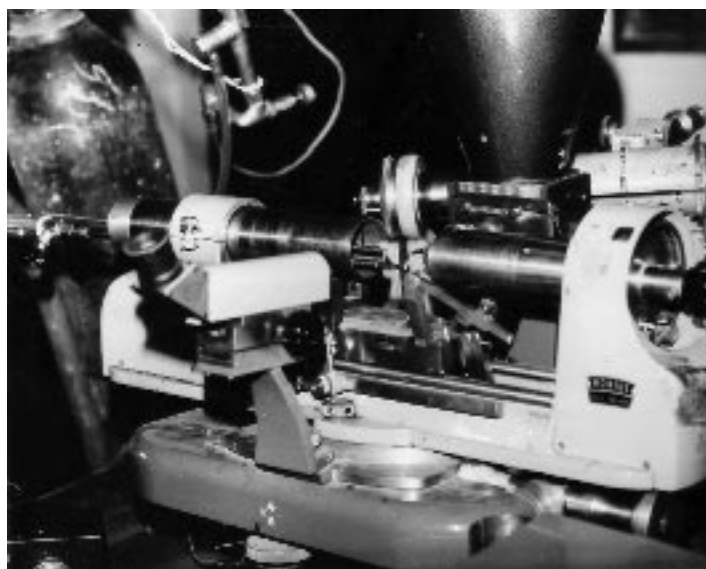


Figure 9: Rotation photograph of MgO at 25°C (1 hr) and 2500°C (20 minutes) (L) Zero level Weissenberg photograph of MgO at 2100°C and 25°C (R) (Exposure time 30 min each).

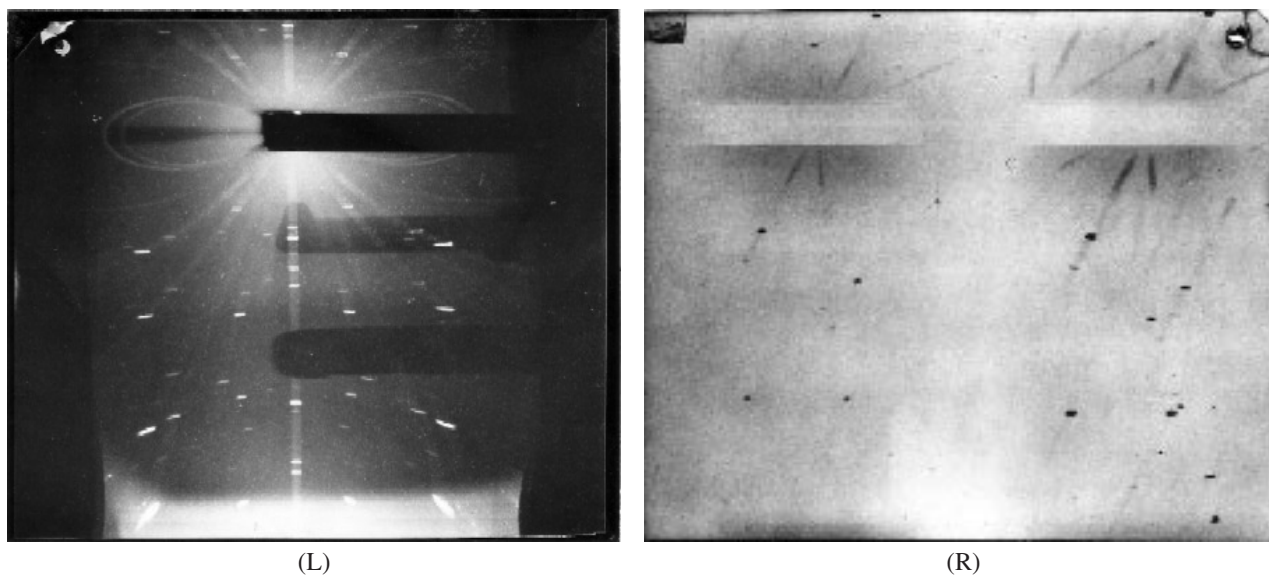


Figure 10: Schematic representation of the furnace assembly: Q quartz rod; P platinum wire heating element; B1, B2, B3 bores in Q; T thermocouple; F1, F2 alumina capillaries carrying thermocouple arms; L1, L2 heater leads; H brass holder in which heating unit is mounted; S height adjusting screw; N1 to and fro adjustment nut; G goniometer head; K experimental crystal mounted inside capillary; J ceramic cement; A alumina cement. Fig.10(b). An isometric view of the furnace assembly mounted on a Buerger's precession camera. R collimator stand; M collimator; B beam stopper; D graduated drum; F level-screen frame; N2 to and for adjustment nut.

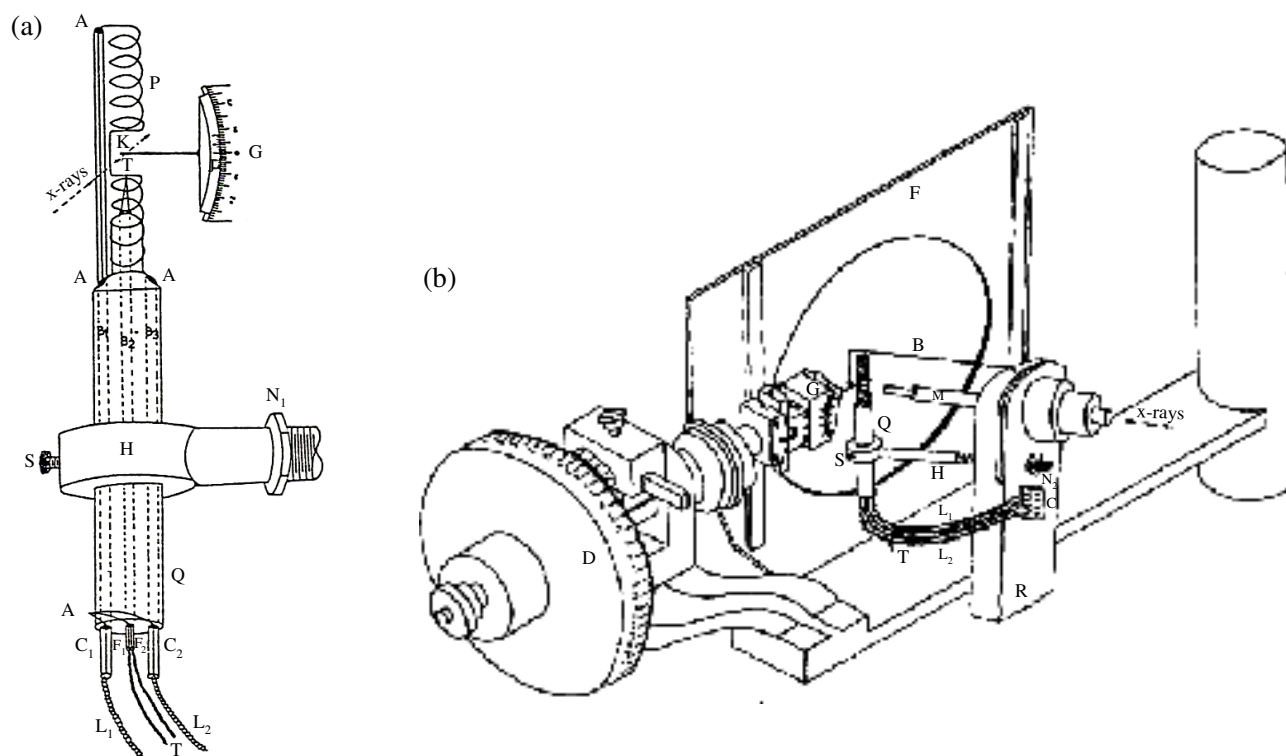
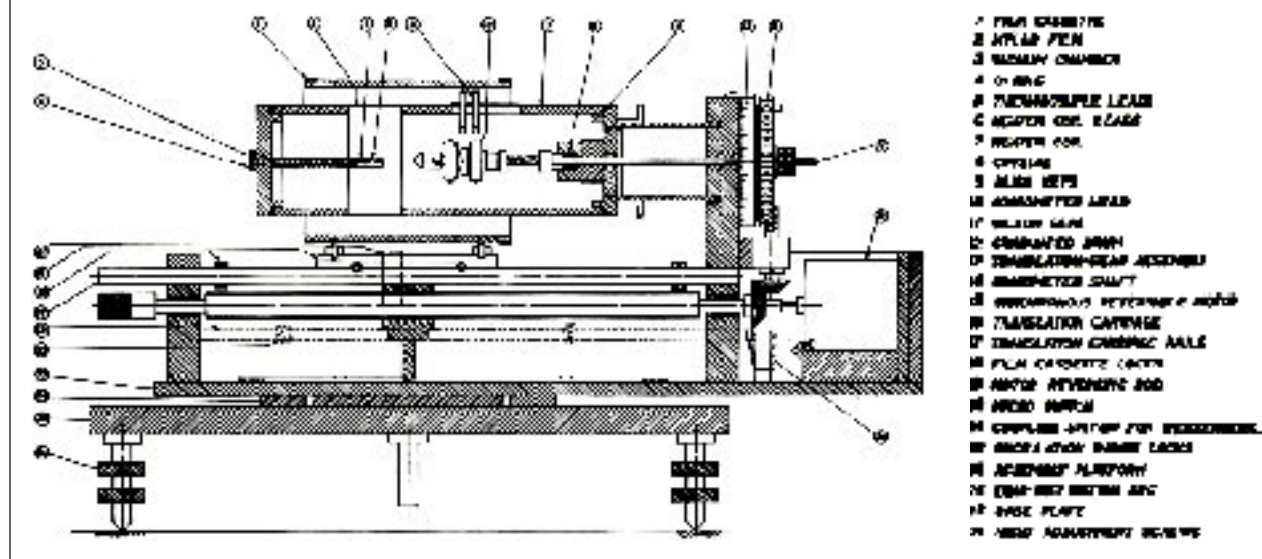


Figure 11: Schematic representation of a complete high Temperature Weissenberg camera.



2.3. A gas flame device suitable for single crystal Weissenberg photography in the temperature range 1000°C–3000°C [8].

Fig. 6. shows the a schematic sketch of the experimental setup. It consists of a fine jet of gas flame A issuing out of a metal nozzle B with a 0.5 mm bore. B is connected to a standard oxy-acetylene regulator C through pipe D, held inside the brass cylinder E. The experimental crystal J is fixed with high temperature cement K in a quartz capillary L mounted on a standard goniometer head M. The crystal is heated is directly heated from the vertical flame issuing out of the nozzle. The temperature of the flame is controlled by regulating the gas flow mixture using the coarse regulators N and the fine control needle valves O. To avoid the possibility of the flame coming in contact with

the film cassette, a long slot (14 cm × 2 cm) is cut in the top of the cassette as shown in fig. 7. The film cassette is also split into two halves, which are hinged on one side as shown in the figure. This is done to eliminate the need for extinguishing the flame and for the removal of the regulator-blow pipe every time the cassette is mounted on or removed from the camera, whenever a new x-ray photograph is to be taken or to be developed. The device has been used for taking single crystal rotation and Weissenberg photographs of MgO (figs. 8 and 9). No water cooling is needed even at highest temperature. The goniometer remains cold since the lateral temperature drop from the flame is extremely high. However, substances, which react in oxidizing and reducing flames and those react with water liberated in the film, cannot be investigated.

Figure 12: Vacuum chamber of the high temperature Weissenberg camera shown in fig. 11.

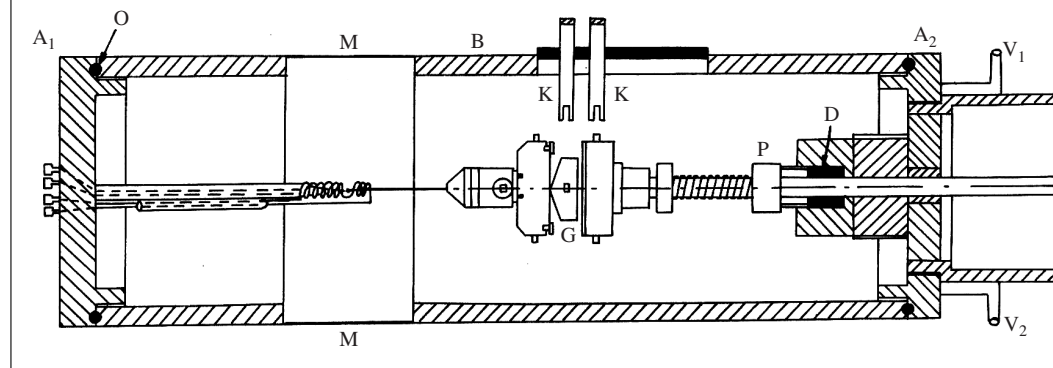


Figure 13: Two views of the high temperature Weissenberg camera, showing vacuum chamber and 114.6 mm dia film cassette.

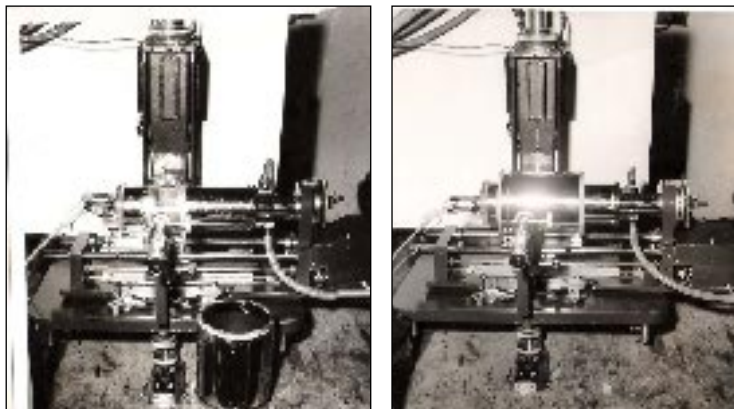
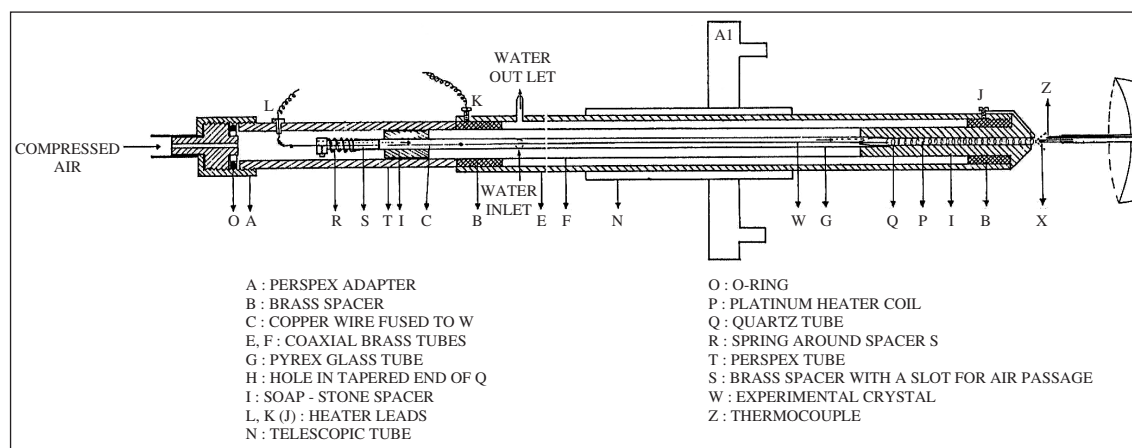


Figure 14: Hot air probe used in high temperature Weissenberg camera.



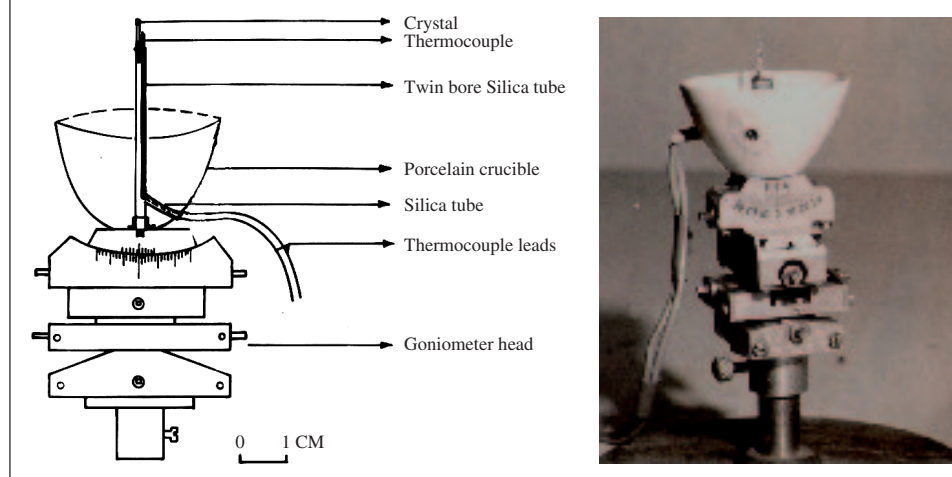
A part of reciprocal lattice falling within the slot provided for flame escape cannot be recorded and investigations at close temperature intervals are difficult.

2.4. A simple heater attachment to precession camera for high temperature diffraction studies up to 1000 °C [9].

The furnace is designed single crystal x-ray diffraction study on Buerger's precession camera. The furnace employs heating of the crystal primarily by radiation from a surrounding current heated platinum coil. The temperature is measured by a built in Pt/Pt-Rh 13% precalibrated thermocouple. It is particularly useful for examining changes in symmetry and crystal data during phase transition, in the range from room temperature to 1000 °C.

A schematic representation of the furnace assembly is given in figure 1. It consists of a quartz rod Q of 6 mm diameter and 3 cm length. A length of 5 mm at one end of the rod, is ground such that it is slightly conical with average diameter of 3 mm. The heater unit, which is fixed on this end of the rod, consists of a platinum wire coil P (30 S.W.G., 25 cm long) split at the centre to provide a 4 mm gap for sample insertion and x-ray irradiation. Rod Q has three bores B1, B2, B3 each of 1 mm diameter. The central bore B2, which is coaxial to the furnace coil carries, a Pt/Pt-Rh 13% thermocouple T, and the tip of which just projects into the x-ray gap. The entire heating unit is mounted in a brass holder H attached to the collimator stand, below the collimator as shown in figure 2. The screw S is provided to adjust the height of heating element

Figure 15: Mounting of experimental crystal for hot air probe.



so that the experimental crystal K lies at the centre of the x-ray gap. Taking care to avoid possible air currents in the x-ray room the temperature of the specimen can be kept constant to $\pm 2^\circ\text{C}$ at 550°C with $\mu = 30^\circ$ for several hours. At 800°C , the power consumed is about 45 watts.

The main feature of this device is its simplicity in construction and use. As it is totally independent of the goniometer head and collimator, crystal mounting and alignment at high temperatures can be done as freely as at room temperature. With the layer-line screen gap covered by thin Mylar film, the temperature of the x-ray film is essentially unaffected up to a crystal temperature of 1000°C . Photographs with $\mu = 30^\circ$ can be taken without any interference by the heating unit. It is easy to replace the furnace in case of any damage during the experiment. The furnace has been used to study the phase transformation in ferroelectric sodium metavanadate.

2.5. A complete high temperature Weissenberg camera [10–12]

The study of single crystals at elevated temperatures in early seventies were commonly done using commercially available Weissenberg cameras with a suitable high temperature attachments (1–7). There was no report of an entire Weissenberg camera designed and built exclusively for high temperature studies. A complete high temperature camera was therefore designed and constructed in the laboratory. While the general features of this instruments are similar to those of common equi-inclination Weissenberg camera, it has several additional features such as vacuum or inert gas chamber, two types of heater assemblies, one resistance heating

device to be used in vacuum/inert gas atmosphere up to 400°C , another a hot air probe for studied up to 900°C in ordinary atmosphere, film cassette of 114.6 mm diameter, and the translational gear system of $1\text{ mm} : 8^\circ$. Fig. X shows the arrangement and the mounting of the experimental crystal on the goniometer head while using the hot air probe. The top of the goniometer carries a porcelain crucible to avoid heating of the goniometer head and camera parts in the vicinity and a centrally placed twin bore silica tube. One of the bore is used for mounting the crystal in silica capillary or stuck on silica fibre. The other bore carries a Pt/Pt-Rh13% thermocouple such that its tip lies just below the crystal. Advantages of this camera are: Oscillation and Weissenberg photographs with maximum equi-inclination angle $= 30^\circ$ can be taken in the range room temperature to 400°C in vacuum or inert gas atmosphere and up to 900°C in air. The use of film cassette of 114.6 mm diameter provides more accurate measurement of lattice parameters than in ordinary Weissenberg camera. With translational gear system of $1\text{ mm} : 8^\circ$ more than one Weissenberg photograph at different temperatures can be recorded on the same film which helps better comparison of crystal data and intensities. This also eliminates the possible errors in measurements due to shrinkage of film.

2.6. A high temperature furnace for Enraf-Nonius CAD-4 Kappa axis Diffractometer [13]

The furnaces and camera described in sections 2.4 to 2.5 were initially developed to investigate changes in the symmetry and to get intensities in the high temperature phase of the ferroelectric NaVO_3 crystal. A critical analysis of these data

showed the, in order to get reliable positional coordinated and temperature factors of the atoms it was desirable to have more accurate intensities as could be obtained with diffractometer. At this time, around mid seventies Indian Institute of Science acquired a computer controlled Enraf-Nonius CAD-4 Kappa axis diffractometer. Earlier designs of the furnaces reported in the literature were for χ -circle diffractometer either attached to χ -circle or mounted on the goniometer itself. It was difficult to incorporate these designs directly into CAD-4 diffractometer, in view of its new geometry where the χ -circle was replaced by movement about an axis called κ -axis. In this geometry the space above

the goniometer head is free from any obstructions. It was felt easy, therefore, to adapt a heater attachment independent of goniometer head or diffractometer circles. A high temperature attachment suitable for routine collection of X-ray data up to 500 °C on Enraf-Nonius CAD-4 kappa axis diffractometer (fig. 19) was designed and fabricated. It was first high temperature furnace made for CAD-4 and remained only design until Enraf-Nonius came up with their design. The furnace consists of a platinum wire wound furnace with a gap for sample insertion and X-ray irradiation. The furnace is totally independent of crystal mounting and therefore crystal centering and interchange can be done as freely as in room

Figure 16: Complete experimental set-up of high temperature Weissenberg camera.



Figure 17: A high temperature furnace for Nonius-Enraf CAD-4 diffractometer up to 500 °C.

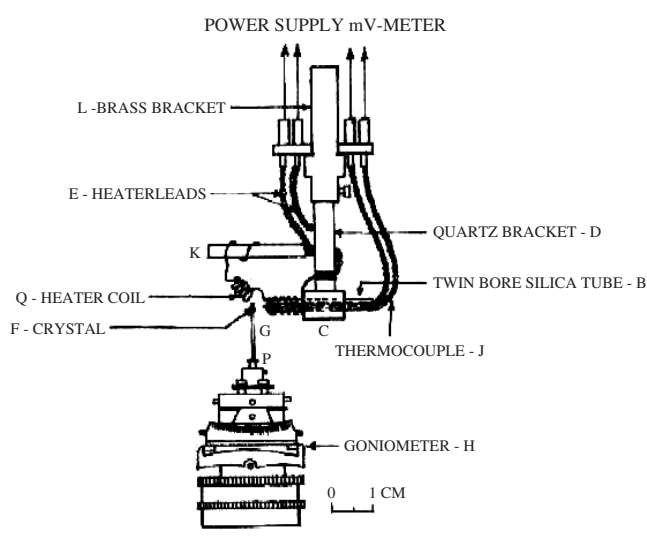


Figure 18: Furnace mounted on the Enraf-Nonius CAD-4 diffractometer.

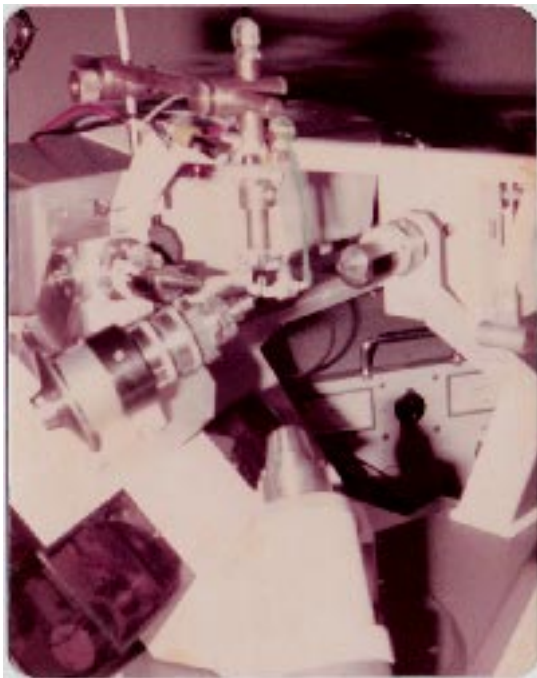


Figure 19: A polaroid photograph of NaVO_3 single crystal at 425°C taken on Enraf-Nonius CAD-4 diffractometer.

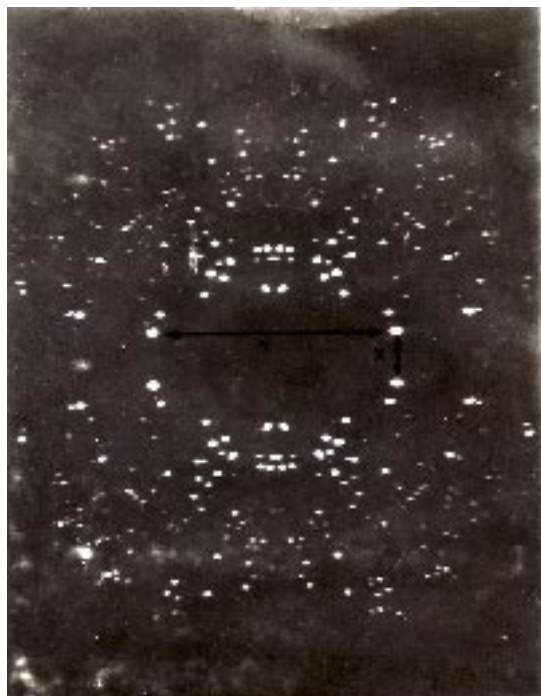
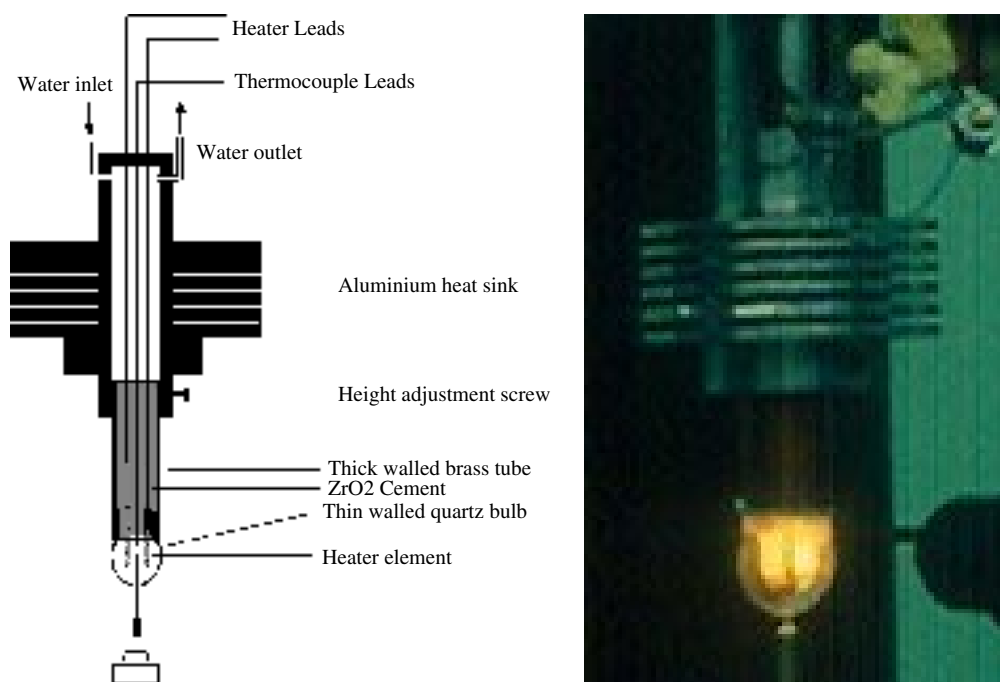
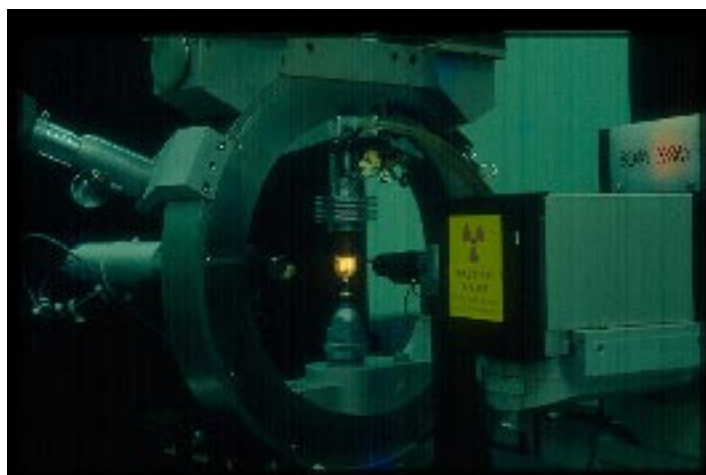


Figure 20: Schematic view of crystal heater (left) and photograph of heater in operation (right).

Figure 21: Photograph of heater assembly attached to the χ -circle of a Syntex P1 4-circle diffractometer.

temperature case. The heater coil and thermocouple can be easily replaced in case of damage. The design of furnace does not obstruct movement of the diffractometer circles during the data collection except the movement of kappa axis is limited up to $\pm 100^\circ$. The furnace has been extensively used to collect thermal expansion and X-ray intensity data from NaVO_3 , Ti_2O_3 , V_2O_3 -doped Ti_2O_3 and CsCuCl_3 single crystals at various temperature.

2.7. A single crystal high temperature attachment for Four Circle X-ray Diffractometer [14].

A single crystal heater attached to the χ -circle of Syntex P1 computer controlled four-circle X-ray diffractometer was fabricated for high temperature investigations of minerals up to 1200°C . It is radiant type platinum electric resistance heater enclosed inside a thin quartz bubble, which acts as a heat shield (fig.). The heater assembly is mounted in

Figure 22: A view of the infinite chain of VO_4 tetrahedra along the c -axis. Only one chain is shown for clarity.

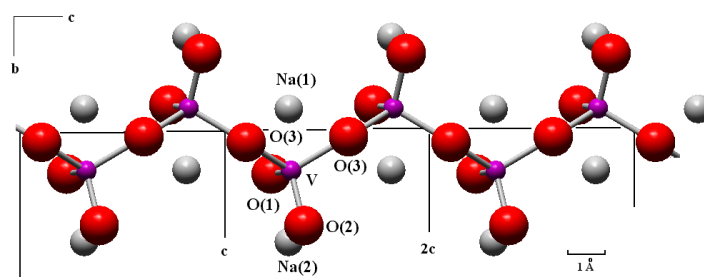
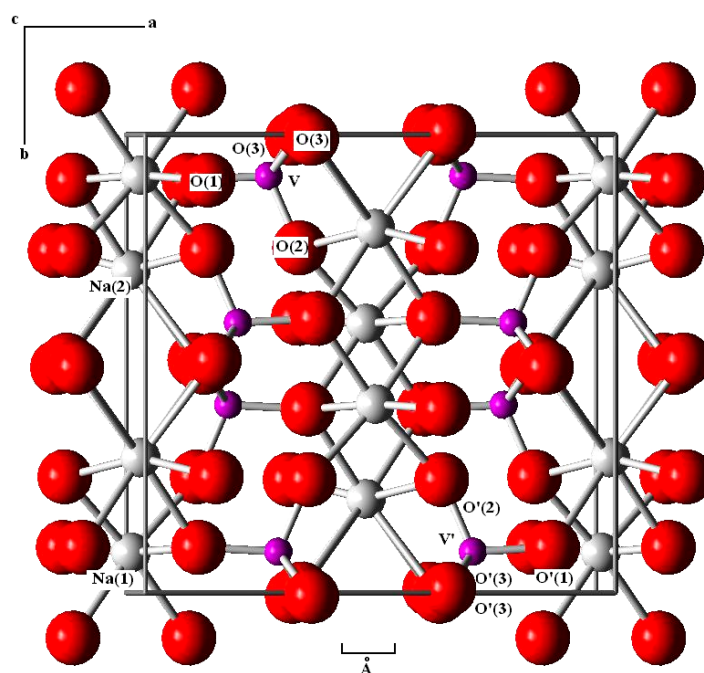


Figure 23: Structure of NaVO_3 looking down the $[001]$ direction.



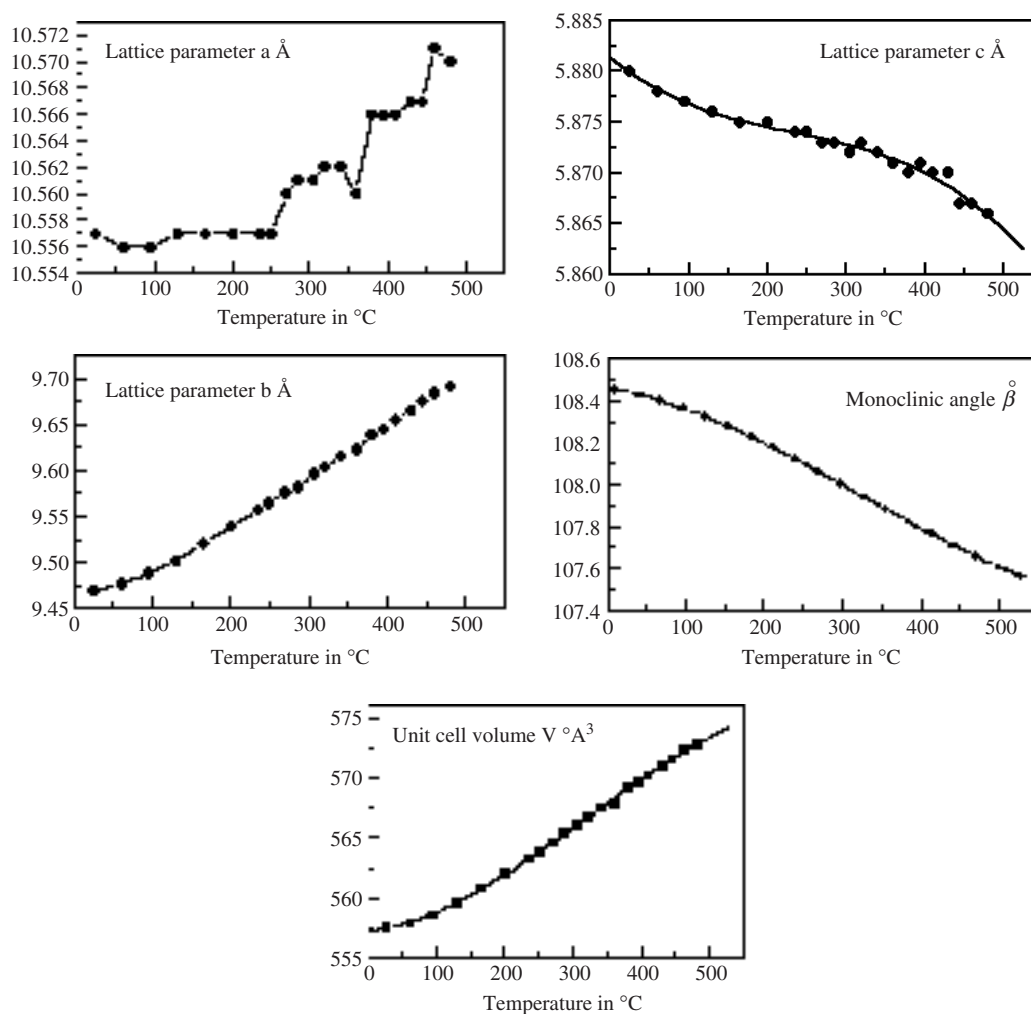
a water cooled telescopic assembly which can be lower easily such that the crystal lies in the centre of heating gap between the two arms of the heater. A tiny hole on the head of the quartz bulb is provided for crystal entry. The temperature is measured with a Pt/Pt-13%Rh thermocouple, tip of which lies in the heating very close to the crystal position. The Heater assembly is attached to the χ -circle facing the ϕ -circle (fig.). The crystal mounted inside quartz capillary is mounted in the goniometer with appropriate high temperature cement and is centered and aligned. Slight misalignment that occurs during heating of the crystal can be adjusted in situ by observing through the microscope of the diffractometer. The power to the heater is provided

by a stable low volts- high current DC supply. Power of approximately 50 watts was adequate for the maximum operating temperature of 1200°C . The heater attachment was used for high temperature study of minerals like albite, zektzerite etc.

3. Some investigations on high temperature Single Crystal X-ray Diffraction

3.1. Crystallographic study of ferroelectric transition in sodium metavanadate, NaVO_3

Among the alkali metavanadates known to exist, ferroelectricity has been found only in case of sodium metavanadate, it shows a. domain pattern and a dielectric hysteresis loop, characteristic of a

Figure 24: Variation of Lattice parameters NaVO_3 with temperature.

ferroelectric below 380 °C [15]. A detailed X-ray analysis of this compound in both the ferroelectric and paraelectric phases was undertaken to study the structural changes that take place during this phase transition. The early part of this work was done photographically using the high temperature set-ups described in paragraphs 2.4 to 2.5 [16]. Finally, the entire analysis was done by collecting the X-ray intensity data on the CAD-4 diffractometer using the high temperature equipment described in para 2.6 [17–18]. Thermal expansion of NaVO_3 from room temperature up to 500 °C, well beyond its transition temperature is also recorded [17].

NaVO_3 belongs to the pyroxene family and isostructural with diopside, $\text{CaMg}(\text{SiO}_3)_2$ where parallel SiO_3 chains are held together by metal ions lying between them. The crystal structure of NaVO_3 consists of infinite VO_3^- chains formed by VO_4 tetrahedra, sharing two corners with each

other. These chains are held together by sodium ions and parallel to the c -axis as shown in Fig. 22. Each sodium is surrounded by six oxygen forming nearly a regular polyhedron. The packing diagram viewed down the c -axis shown in fig. 23. The crystal structure may be viewed as consisting of alternate channels of sodium polyhedra and linear chains of VO_3^- ions.

In our high temperature work the high temperature structure of NaVO_3 at 425 °C is found to be essentially the same as that at room temperature [Tables 1–3]). However, some significant changes are found in the orientation of the thermal ellipsoids of the atoms and their thermal amplitudes. It can be seen that on heating, the thermal amplitudes in general, show an increase of 50%. The vanadium and oxygen atoms V and O_3 , which are linked in the VO_4 tetrahedral chain show a somewhat lesser increase compared to other atoms.

Thermal Ellipsoids of vibration of atoms:

Principal axes of vibration ellipsoids and their direction cosines wrt crystallographic axes a , b , c were calculated from anisotropic temperature factors obtained from structure refinement. Comparison of the thermal ellipsoids in both the phases shows that

1. On heating the increase in thermal amplitudes in Na(1) and Na(2) atoms is significant along all three principal directions.

	Na(1)		Na(2)	
1	0.161 Å	0.240	0.220	0.341
2	0.130	0.195	0.144	0.232
3	0.089	0.141	0.107	0.153

2. Vanadium atom which has almost isotropic vibrations at RT becomes highly anisotropic at HT.
3. Several atoms show maximum amplitude of vibrations almost Along b -axis on heating,

	Inclination With b -axis	u
Na(1)	30.61 °	0.240 Å
V	10.55	0.201
O(1)	7.31	0.235
O(3)	14.60	0.292

This feature is consistent with the observation that maximum thermal expansion of NaVO₃ occurs along the b -axis.

4. The orientation of the principal vibration amplitudes of V and O(3) atoms wrt to crystallographic axes, are similar. They also have least vibrations along c direction which is consistent with the fact that V and O(3) are linked together to form a VO₄ chain running along the c -axis.

NaVO₃ does not undergo any drastic change of crystal structure on heating. If the ferroelectric transition takes place at 380 °C as reported it does

Table 1: Crystal Data of NaVO₃

NaVO ₃ , M.W. 121.94	
25 °C	425 °C
$a = 10.557(2)$ Å	10.570(2)
$b = 9.469(3)$	9.692(3)
$c = 5.880(1)$	5.866(1)
$\beta = 108.43(2)^\circ$	107.63(2)
$V = 557.65$ Å ³	572.66
$Z = 8$	4
Monoclinic Cc	Monoclinic C2/c
R-factor 3.6	4.5

not seem to be accompanied by any drastic change in the crystal structure. It is probably connected with, among other factors the changes in nature of the thermal ellipsoids of vibration of atoms. The lattice parameter a varies from 10.557(2) Å at room temperature to 10.570(2) Å at 480 °C; and shows an anomalous behaviour in the temperature range 360–380 °C. The thermal expansion is maximum along b -axis; it expands from 9.469(3) Å at room temperature to 9.692(2) Å at 480 °C. The c and β parameters, however, decrease with temperature from 5.880(1) Å to 5.866(1) Å and 108.43(2) ° to 107.63(2) °. The unit cell volume, expands from 551.65 Å³ to 572.66 Å³, the increase in the vicinity of the transition temperature (340–400 °C) is about 0.5%. The thermal expansion anomaly observed along the a -axis [fig. 24] is consistent with the irreversible dielectric anomaly along $[a \sin \beta]$ direction reported in literature [19].

3.2. Semiconductor to metal transition in Ti₂O₃ and V₂O₃-doped Ti₂O₃[20]:

Ti₂O₃ undergoes a semiconductor–metal transition around 400 K without any accompanying change in crystal symmetry [21, 22]. The transition is, however, accompanied by a change in the c/a ratio. The transition is considered to be due to the crossing of a_l and e_π bands with increase in temperature [23]. All the recent studies on the Ti₂O₃ transition are in conformity with this mechanism. According to this mechanism, the Ti–Ti distance along the three-fold axis should increase with temperature while the opposite would be true for the Ti–Ti distance in the basal plane. Doping of Ti₂O₃ by V₂O₃ progressively reduces the magnitude of the conductivity jump, until at 10% V₂O₃, the material is metallic [24]; the lattice parameters of 10% V₂O₃-doped sample are reported to be close to those of the high temperature metallic phase of Ti₂O₃[25–26]. We have carried out detailed crystallographic studies of pure Ti₂O₃ and also of Ti₂O₃ doped with V₂O₃. The study shows expected variations in Ti–Ti distances and other structural parameters with temperature. We consider these studies important in understanding the mechanism of the semiconductor-metal transition in Ti₂O₃ and the mode of action of the V₃⁺ impurity.

Single crystals of Ti₂O₃ and V₂O₃-doped Ti₂O₃ were mounted on the goniometer head of an Enraf-Nonius CAD-4 diffractometer. A high temperature attachment described in 2.5 was used for the study of Ti₂O₃. Variations of the lattice parameters of Ti₂O₃ with temperature and also with the incorporation of V₂O₃ are shown in Fig. 1. We see from the figure that the lattice parameter variations in the two cases are not exactly identical. Thus, the unit cell

Table 2: Fractional Coordinates of atoms in NaVO₃

Atom	RT			425 °C		
	x	y	z			
Na(1)	0	0.9124(0)	0.25	0	0.9094(8)	0.25
Na(2)	0	0.2941(1)	0.25	0	0.2943(10)	0.25
V	0.2921(0)	0.0898(0)	0.2612(1)	.2925(2)	.0883(2)	.2593(3)
O(1)	0.1283(2)	0.1010(2)	0.1689(0)	.1287(10)	.0984(10)	.1651(19)
O(2)	0.3566(2)	0.2463(2)	0.3257(4)	.3568(12)	.2429(13)	.3207(19)
O(3)	0.3532(2)	0.0084(2)	0.0386(3)	.3515(9)	.0068(14)	.0318(16)
V'	-.2923(0)	-.0898(0)	-.2615(1)			
O'(1)	-.1263(2)	-.1013(2)	-.1683(3)			
O'(2)	-.3565(2)	-.2492(2)	-.3219(4)			
O'(3)	-.3524(2)	-.0066(2)	-.0375(3)			

ESD's are given in parantheses

volume of Ti₂O₃ increases with temperature (just as the c/a ratio), in contrast to the earlier report in the literature [27]. The present observation of volume increase during the transition seems to explain the absence of pressure effect on the Ti₂O₃ transition [28]. With the incorporation of V₂O₃, however, the unit cell volume decreases. This may be because, a_{hex} as well as α vary more steeply with % V₂O₃ than with increasing temperature. The detailed structural parameters of V₂O₃-doped Ti₂O₃ samples are given in Table 4. For the purpose of comparison, the data on the high temperature phase of Ti₂O₃ are also given.

In the crystal structure of Ti₂O₃ [29] which is isomorphous with corundum structure (fig. 26), a given Ti atom, M₁ has four near Ti neighbors: one M₂, sharing a face of the oxygen octahedron, and three M₃, sharing edges of the octahedron [28]. We see from Table I that incorporation of V₂O₃ results in an increase in the M₁-M₂ distance across the shared octahedral face (just as with increase in temperature) from 2.582 Å in Ti₂O₃ to 2.658 Å in 10% V₂O₃ doped Ti₂O₃. This increase in M₁-M₂ is accompanied by an increase in the c -parameter and in the distance of M1 from the O1-O3 plane perpendicular to this axis. Doping with V₂O₃ also

causes a decrease in the M₁-M₂ distance from 2.994 Å in pure Ti₂O₃ to 2.968 Å in 10% V₂O₃-doped sample (Fig. 27); this decrease in the Ti-Ti distance in the basal plane is accompanied by a decrease in the a parameter. The M-O distances vary only slightly, but we do notice a significant variation in the M₁-O₁-M₂ angle from 77.30° in pure Ti₂O₃ to 79.79° in the 10% V₂O₃-doped sample. Other angles, which show significant variations, are: O₁-M₁-O₂ and O₁-M₁-O₆ (decrease), O₁-M₁-O₅ (increase). The distances from M₁ (as well as O₄) to the O₁-O₃ plane also increase with incorporation of V₂O₃. Decrease in a_{hex} with % V₂O₃ is consistent with the reduction in the O₁-O₂ distance.

The results of the present study show that the electronic properties of V₂O₃-doped Ti₂O₃ can be explained by the band broadening mechanism of Van Zandt, Honig and Goodenough [23]. More specifically, the study confirms that the two narrow d-bands cross each other following variations in the crystallographic c/a ratio [30].

3.3. Jahn-Teller effect induced phase transitions in CsCuCl₃ [31]

The room-temperature structure of CsCuCl₃ (P6₁22 or P6₅22; $a = 7.22$ Å, $c = 18.18$ Å) consists of hexagonally close-packed layers of cesium and chloride ions with three unequal Cu-Cl distances in the CuCl₆ octahedron; the Cu atoms are 0.42 Å from the 6_1 - c axis and form spiraling chains by sharing faces of octahedra [32]. CsCuCl₃ undergoes a first-order phase transition at 423 K to a more symmetrical phase ($a = 7.26$ 2Å, $c = 6.20$ Å) with a reduction of the c -parameter to one third of the parent structure [33,34]. The high temperature structure is reported to be isomorphous with that of CsNiCl₃ (P6₃/mmc) and the transition is attributed to the cooperative Jahn-Teller effect [35]. It has been reported that CsCuCl₃ undergoes two additional transitions at 511 K and 535 K

Table 3: Comparison of isotropic temperature factors B and thermal amplitudes u in NAVO₃

Atom	B (Å ²)		u (Å)	
	RT	HT	RT	HT
Na(1)	1.410	2.707	0.134	0.185
Na(2)	1.702	3.661	0.147	0.215
V	0.987	1.907	0.112	0.155
O(1)	1.368	3.224	0.132	0.202
O(2)	1.868	3.698	0.154	0.217
O(3)	1.643	2.872	0.144	0.191

B calculated from anisotropic temperature factors b_{ij} using Hamilton's equation (1959)
 $B = 4/3 \sum \sum b_{ij}(a_i a_j) = 8\pi^2 u^2$

Table 4: Fractional coordinates and temperature factors of metal atoms and bond distances in Pure and V₂O₃-doped Ti₂O₃ structure (space group: R $\bar{3}c$)

Metal atom:						
Parameters	Pure Ti ₂ O ₃ RT	Ti ₂ O ₃ + 0.5 % V ₂ O ₃	Ti ₂ O ₃ + 2% V ₂ O ₃	Ti ₂ O ₃ + 4% V ₂ O ₃	Ti ₂ O ₃ + 10% V ₂ O ₃	Pure Ti ₂ O ₃ HT 580 K
$x = y = z$	0.34475(2)	0.34483(3)	0.34515(2)	0.34556(3)	0.34596(3)	0.34607(3)
$b_{11} = b_{22} = b_{33}$	0.0039(2)	0.0030(4)	0.0044(2)	0.0047(2)	0.0068(2)	0.0076(1)
$b_{12} = b_{13} = b_{23}$	-.0013(1)	-.0010(2)	-.0014(1)	-.0018(1)	-.0032(1)	-.0027(1)
Oxygen atom:						
Parameters	Pure Ti ₂ O ₃ RT	Ti ₂ O ₃ + 10% V ₂ O ₃	Pure Ti ₂ O ₃ HT 580 K			
x	0.5630(2)	0.5614(3)	0.5618(2)			
y	-0.0630(2)	-0.0614(2)	-0.0618(2)			
z	0.25	0.25	0.25			
$b_{11} = b_{22}$	0.0062(2)	0.0080(4)	0.0102(3)			
b_{33}	0.0050(2)	0.0074(7)	0.0082(4)			
b_{12}	-0.0030(2)	-0.0015(6)	-0.0020(3)			
$b_{13} = b_{23}$	-0.0017(1)	-0.0032(3)	-0.0037(2)			
ESDs are given in parentheses. The temperature factors are of the form $T = \exp-(b_{11}h^2 + . + 2b_{12}hk + \dots)$						
Bond distances						
Bond	Pure Ti ₂ O ₃ RT	Ti ₂ O ₃ + 0.5% V ₂ O ₃	Ti ₂ O ₃ + 2% V ₂ O ₃	Ti ₂ O ₃ + 4% V ₂ O ₃	Ti ₂ O ₃ + 10% V ₂ O ₃	Pure Ti ₂ O ₃ HT 580 K
M1-M2	2.582(1)	2.584(0)	2.602(0)	2.628(0)	2.658(0)	2.657(0)
M1-M3	2.994(0)	2.989(0)	2.982(0)	2.976(0)	2.968(0)	2.982(0)

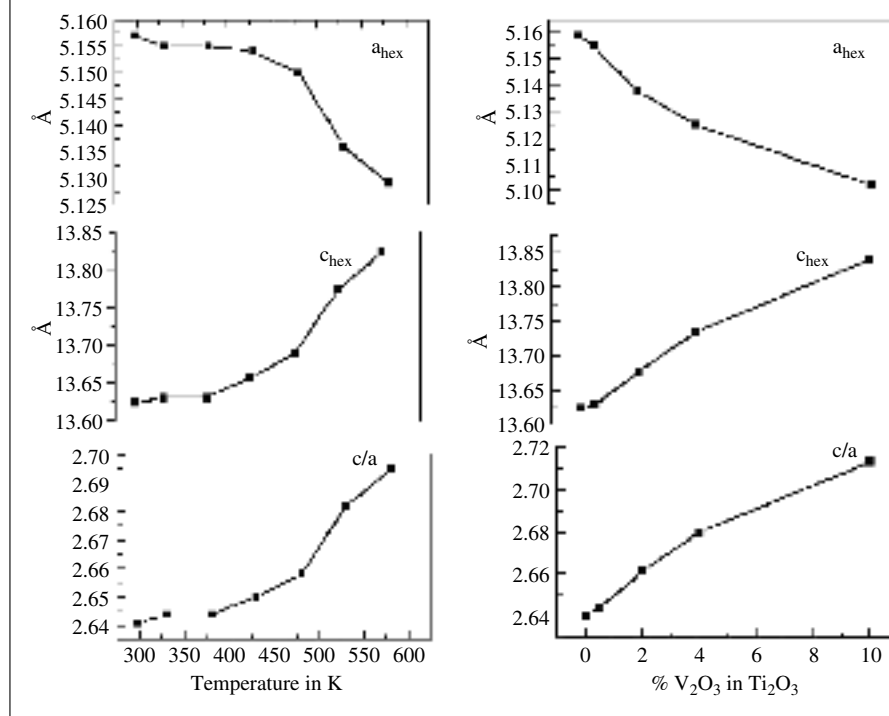
[36]. We have examined these transitions by single crystal X-ray diffraction employing an Enraf-Nonius CAD-4 diffractometer fitted with a high temperature attachment described in para 2.5. The measurements clearly establish the existence of the three transitions at 423, 510, and 535 K as shown in fig. 28 where we have plotted the temperature variation of the unit cell volume as well as the c/a ratio. Our X-ray studies agree with the P6₅22 (P6₁22) group assigned to the room-temperature phase of CsCuCl₃. The three high-temperature phases (after the 423, 510 and 535 K transitions) show similar systematic absences (hh2- $hl:l = 2n$). If we were to assign the centrosymmetric P6₃/mmc space group to the phase after the first-order transition at 423 K as reported in the literature [33,34], the question then arises as to the space groups above the 510 and 535K transitions. In view of the results from our IR studies, we feel that the space group after the 423 K transition is P6₃/mc or P-62c, both of which are non-centrosymmetric and would show similar systematic absences in X-ray diffraction data; this suggestion has also been made by Kroese et al. [33]. Either of these could then transform to P6₃/mmc after the transition at 510 K. The phases after the 510 K and the 535 K

transitions may belong to the same space group probably differing only in positional parameters. These changes in symmetry accompanying phase transitions in a solid like CsCuCl₃ exhibiting antiferrodistortive ordering are indeed interesting.

3.4. A second order phase transition induced by Na⁺-ion order-disorder in Zektzerite, NaLiZrSi₆O₁₅: high temperature single crystal X-ray diffraction studies [37–39].

Zektzerite, NaLiZrSi₆O₁₅ is orthorhombic, space group *Cmca*, with unit cell dimensions: $a = 14.330(2)$, $b = 17.354(2)$ and $c = 10.164(2)$ Å under ambient conditions. Its crystal structure consists of corrugated six-tetrahedral-repeat corner-sharing double silicate chains, interconnected into a three-dimensional framework by edge-sharing chains of alternating [LiO₄] tetrahedra and [ZrO₆] octahedral, both sets of chains running parallel to the c -axis. The sodium atoms occur in cylindrical channels parallel to a formed by the corrugation of the double silicate chains. In addition, there is a nominally vacant Na-site above and below the Zr-octahedra along the a -axis as shown in fig. 29 [39–40]. We expected that at high temperature, some of the Na⁺-ions will migrate from the occupied

Figure 25: Variation of lattice parameters of Ti_2O_3 with temperature (left side) and with doping of V_2O_5 at 298 °K (right side).

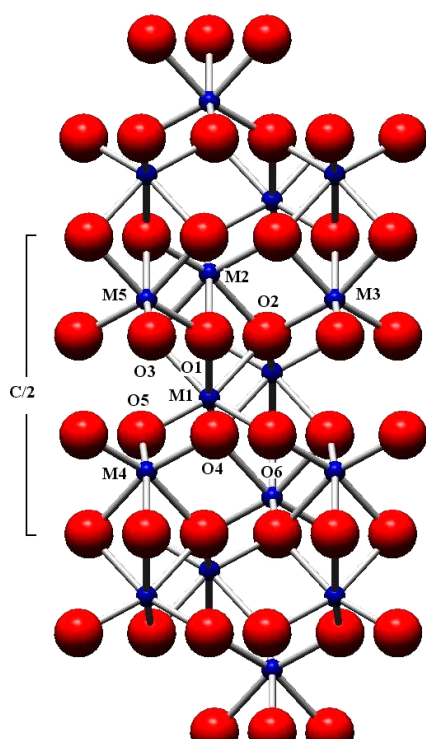
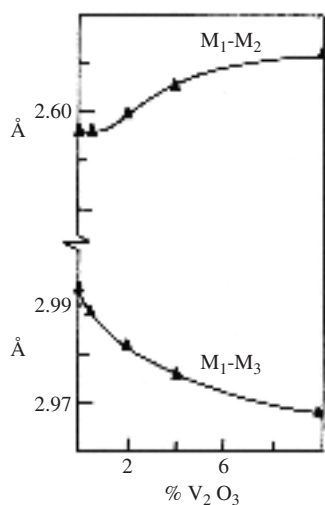


Na(1) site to the vacant Na(2) site. High temperature single crystal X-ray diffraction experiments [41] at 673 and 873 K confirmed the partial migration of the Na^+ -ions from the occupied Na (1) site to the vacant Na (2) site. Electrical ac conductivity (σ) measurements along [100], [010] and [001] as a function of temperature up to 1173 K confirmed this idea [42]. The conductivity measurements along [100] showed activation energy of 1.90 eV on heating, which decreased to 1.64 eV on cooling. Likewise, measurements along [010] showed high temperature activation energy of 1.59 eV; on cooling, after holding the crystal for 15 hrs at 813 K, it was reduced to 1.46 eV and the conductivity increased considerably compared to the values measured on the heating cycle. Similarly, the conductivity measurements along [001] showed activation energies of 1.56 and 1.43 eV on heating and cooling, respectively. The ionic conductivity above 797 K, particularly the significant increase after holding the crystal at 1173 K for 15 hrs, can be correlated with the migration of Na^+ -ions from the occupied Na(1)-site to the vacant Na(2)-site. The lowering of the activation energy barrier during the heating and cooling cycle presumably is due to the creation of vacancies at the fully occupied Na(1)-site under ambient conditions. High temperature single crystal X-ray diffraction experiments on zektzerite

(heating and cooling) up to a temperature of 1373 K were carried out to study crystal structure migration of Na(1) to Na(2) site [37–39].

The single crystal diffraction intensities were collected on a Syntex P computer controlled four-circle X-ray diffractometer, using graphite monochromated $\text{MoK}\alpha$ radiations ($\lambda = 0.7107 \text{ \AA}$). The platinum electric resistance heater attachment described in para 2.6 was used for collecting data at high temperatures. The unit cell parameters were determined at various temperatures from 300 K to 1373 K and then by cooling the crystal from 1373 K to the room temperature. X-ray diffraction intensities at 300 K, 773 K, 973 K, 1223 K and 1323 K were collected. At high temperatures, there is no change in crystal structure of zektzerite; it remains orthorhombic with Cmca space group. The structure at room temperature was refined using previously reported [40] values of atomic coordinates and temperature factors of zektzerite. The structure at 773 K was refined using the room temperature refined parameters. The parameters resulting from one high temperature structure refinement were used for the next high temperature structure refinement. This is an efficient and fast procedure to follow the thermal evolution of the various structural parameters. At room temperature the structure refinement was carried out with full

Figure 26: The corundum structure viewed along a axis of the hexagonal cell.

Figure 27: Variation of Ti-Ti distance in Ti_2O_3 with incorporation of V_2O_3 at 298 K.

occupancy of Na(1) position, while Na(2) position was kept vacant. At high temperatures both Na(1) and Na(2) occupancies were refined keeping total occupancy as 1.0. The crystal structures of zektzerite 300 K, 773 K, 973 K, 1223 K and 1323 K were refined based on 2236, 2113, 2041, 1818 and 1205

independent X-ray reflections to R -factors of 0.038, 0.043, 0.045, 0.053 and 0.057, respectively.

The thermal expansion of zektzerite in terms of unit cell dimensions and unit cell volume up to 1373 K are shown in fig. 30. On heating, a definite change occurs in the slopes of the thermal expansion

Figure 28: Plots of unit cell volume, V_u (full line), and c/a ratio (dotted line) of CsCuCl_3 , against temperature (K) showing three phase transitions.

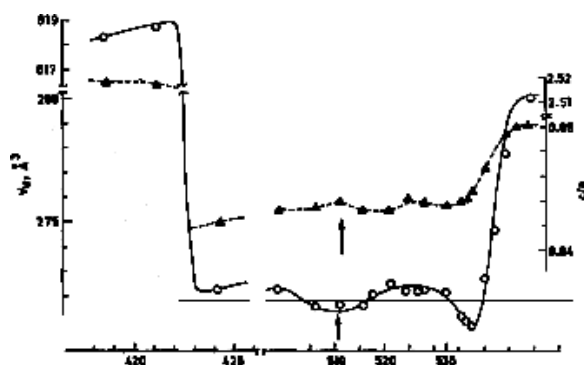
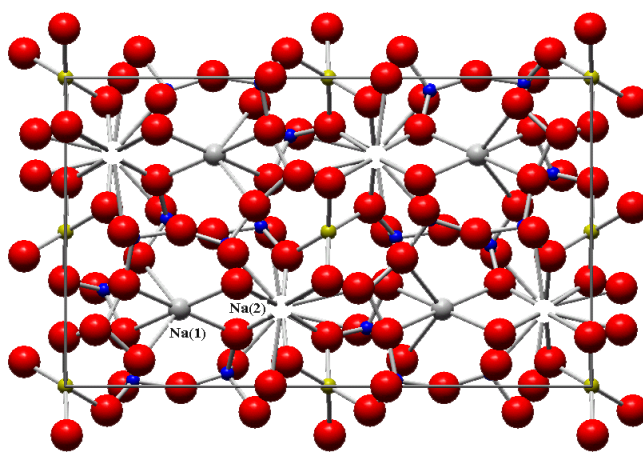


Figure 29: View of The $\text{NaLiZrSi}_6\text{O}_{15}$ structure down [100]. The vacant position which lies above the Zr atom is shown by an open circle.



curves along a , b and c at 1123 K. Furthermore, the thermal expansion curve of c shows an inflection at 623 K. On cooling, a marked hysteresis effect is observed for a , b and c , which is particularly pronounced for b . The thermal expansion along a and b are linear on cooling, whereas c shows inflections at 1123 and 623 K.

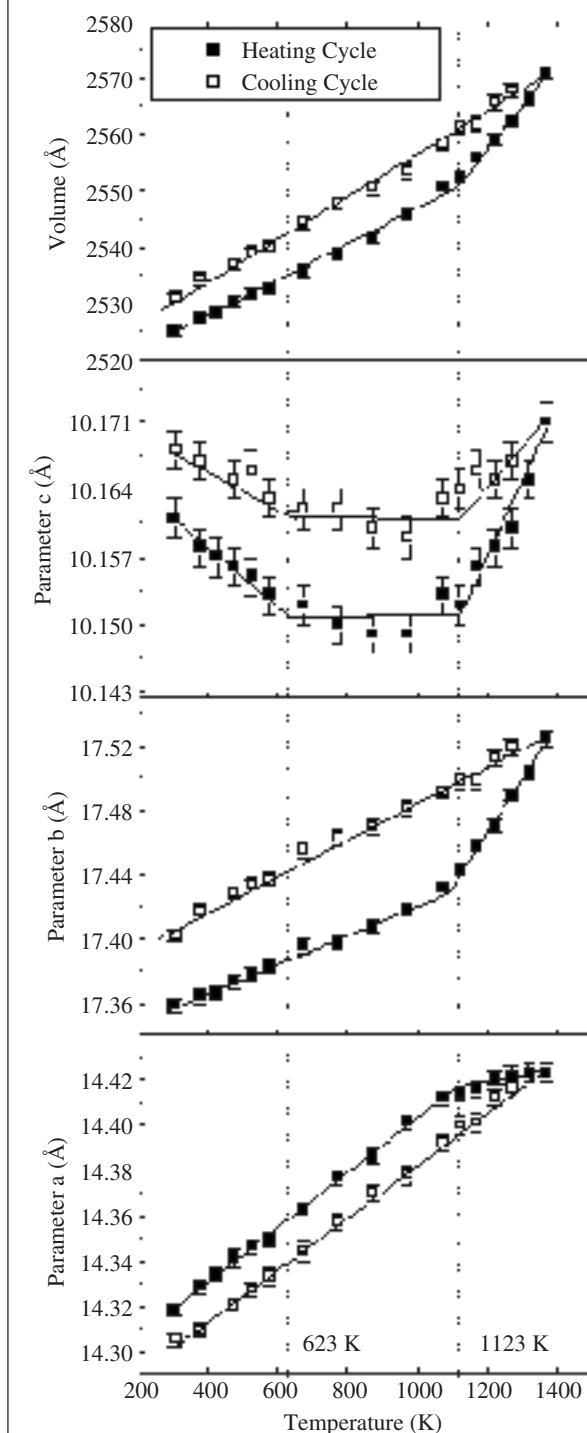
The thermal response of the crystal structure is manifested in two different ways: (a) anisotropic thermal expansion of the cation polyhedra, particularly, the $[\text{LiO}_4]$ tetrahedra and the Na-polyhedra and (b) increasing disorder of the Na^+ -ion, migrating from the occupied Na(1) site to the Na(2) site, the latter being nominally vacant under ambient conditions. On a short time scale (hrs), the first effect is nearly reversible, whereas the second one is only partially reversible. The sodium occupancy at the Na(2)-site increases from 0 at RT

to 0.40 at 773 K, 0.070 at 973 K, 0.13 at 1223 K and 0.35 at 1323 K (fig. 31). Refinement of the crystal structure at RT after heating (up to 1373 K) and cooling cycle indicates a residual sodium content at the Na(2)-site of 0.04. Clearly, the hysteresis effect observed in the thermal expansion behavior on heating and cooling is primarily due to the Na^+ -ion order-disorder as a function of temperature.

The ten-coordinated Na(1) polyhedron is the most sensitive to temperature. The three pairs of shorter bonds involving O(3), O(5) and O(6) (2.37 to 2.76 Å) increase with increasing temperature, whereas the two pairs of relatively longer bonds involving O(1) and O(1') (3.12 to 3.23 Å) decrease, resulting in a more regular polyhedron at high temperature.

The $[\text{LiO}_4]$ tetrahedron also shows considerable thermal expansion, the two sets of Li-O bonds

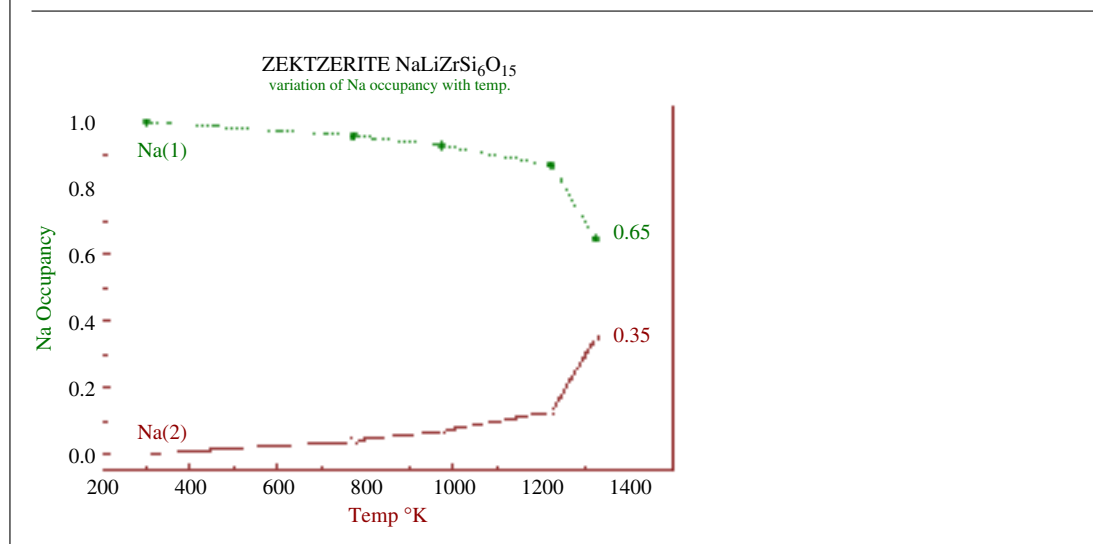
Figure 30: The thermal expansion of unit cell dimensions of Zektzerite up to 1373 K.



increasing from 1.958 and 1.963 Å at RT to 2.030 and 2.088 Å at 1323 K, respectively. In contrast, the [SiO₄] tetrahedron and [ZrO₆] octahedron do not significantly change with temperature. However, the significant thermal changes in the size and configuration of the [LiO₄] tetrahedron and

[NaO₁₀] polyhedron and the thermal expansion of the unit cell dimensions are principally effected by the increase in the Si–O–Si angles at the linkages between two adjacent tetrahedra in the silicate double chains. There are two types of Si–O–Si angles: (a) involving oxygen atoms lying on mirror planes

Figure 31: Conduction of Na atoms from occupied position Na(1) to vacant position Na(2) as function of temperature.



connecting two single silicate chains across the mirror plane into double chains, namely, O(7), O(8) and O(9) with an average Si-O-Si angle of $155.7 \pm 4.2^\circ$ at RT and, (b) involving oxygen atoms O(1), O(3) and O(5) within a single silicate chain with an average Si-O-Si angle of $147.6 \pm 0.6^\circ$ at RT. The difference between the two sets of Si-O-Si angles decreases with increasing temperature from 7.9° at RT to 5° at 1323 K. Essentially, these changes in the silicate chain configurations result in a more regular cavity around the Na(1) atom at high temperature.

The electrical conductivity is highest along [001], intermediate along [010] and least along [100]. The Na(1)-Na(1) conduction along [001] is most favored after partial vacancies are created at this site because the the Na(1) polyhedron shares two opposite edges [O(1)-O(1')] with adjacent Na(1) polyhedra to form a chain parallel to [001] and the nearest Na(1)-Na(1) distance is 5.21 Å at RT (see Fig. 1(a) in [48]). Although the Na(1)-Na(2) distance along [010] is shorter (3.62 Å at RT), the ionic conduction along this path is less favored due to the fact that the Na⁺ ions must pass through one of two rhombus-shaped bottlenecks [formed by O(2)-O(3)-O(4)-O(4') and O(4)-O(5)-O(6)-O(2)], that are narrower than those along [001]. The conduction along [100] is least favored due to the long Na(1)-Na(1) distance (7.17 Å at RT) along this path.

The high electrical conductivity along [001] resulting from higher ionic conduction along this path is consistent with the anisotropic thermal vibration of the Na(1) atom, the longest axis of the thermal vibration ellipsoid lying 32° from

the *c*-axis in the *a*-*c*-plane at RT. A change in the conduction mechanism above 799 K is indicated by a change in the activation energy. Above 1123 K, the electrical conductivity substantially increases due to the substantial migration of Na⁺ ions from the filled Na(1) to the vacant Na(2) site, coinciding with the second order phase transition.

Received 24 July 2007; revised 06 August 2007.

References

1. W.H. Bragg, *Phil. Mag.*, 27, 881, 1914.
2. J.H. Goldschmidt, 'High Temperature X-ray Diffraction Techniques', International Union of Crystallography, Commission of Crystallographic Apparatus 1964.
3. W.J. Campbell, 'Hand Book of X-rays' edited by E.M. Kaelble, Chapter 13, New York: McGraw-Hill, 1967.
4. F.V. Schossberger, 'Hand Book of X-rays' edited by E.M. Kaelble, Chapter 14, New York: McGraw-Hill, 1967.
5. M.A. Viswamitra, A.M. Shaikh and K. Jayalakshmi Ramanuja, 'High temperature X-ray crystallography: Devices for single crystal analysis', *J. Ind. Instt. Sci.*, 57(1), 1-19, 1975.
6. M.A. Viswamitra, K. Jayalakshmi And V. Kalyan1, A miniature furnace for X-ray Weissenberg photography up to 1000 °C, *J. Appl. Cryst.* 3, 227(1970).
7. M.A. Viswamitra and K. Jayalakshmi, A simple miniature furnace for routine collection of single crystal X-ray data up to 1000 °C on the Hilger and Watts linear diffractometer, *J. Phys. E. (J. Sci. Instr.)* 3, 656(1970).
8. M.A. Viswamitra and K. Jayalakshmi, Flame technique for high temperature single crystal Weissenberg photography (1000-3000 °C), *Advances in X-ray analysis*, New York, Plenum Press, 15, 548(1972).
9. A.M. Shaikh and M.A. Viswamitra, A simple heater attachment to precession camera for high temperature diffraction studies up to 1000 °C. *Pramana* 1(4), 204-7, 1973.
10. A.M. Shaikh and M.A. Viswamitra, A high temperature Weissenberg camera for single crystal X-ray diffraction studies. National Conference On Crystallography, I.I.Sc., Bangalore, G1, 1974.

11. A.M. Shaikh and M.A. Viswamitra A hot air probe for high temperature single crystal X-ray diffraction studies., National Conference on Crystallography, NPL, New Delhi, K13, 143, 1975.
12. A.M. Shaikh and M.A. Viswamitra, A High Temperature furnace for Enraf-Nonius CAD-4 kappa axis diffractometer, National Conference on Crystallography, University of Madras, January 17–21, 1977, D-12, p.28.
13. A.M. Shaikh, 'Investigations in High Temperature Single Crystal X-ray Crystallography' Ph.D. Thesis, Indian Institute of Science, Bangalore, 1979.
14. A.M. Shaikh and S. Ghose, Private Communication, 1984.
15. S. Sawada and S. Nomura, J. Phys. Soc. Japan, 6, 192, 1951
16. K. Ramani, A.M. Shaikh, B.S. Reddy and M.A. Viswamitra, Crystal structure of ferroelectric sodium metavanadate, NaVO_3 , Ferroelectric 9, 49–56, 1975.
17. A.M. Shaikh, M.A. Viswamitra and P.S. Narayanan, Thermal expansion and phase transition in NaVO_3 , Ferroelectric, 20, 313, 1978.
18. A.M. Shaikh Crystal chemistry of pyroxene vanadates: Crystal structure refinement, Na anisotropy and rigid body analysis of thermal vibrations in ferroelectric NaVO_3 , Ferroelectrics, 107, 219–224, 1990.
19. M. Matsuda, J. Phys. Soc. Japan, 36, 759, 1974.
20. A.M. Shaikh, M.A. Viswamitra and C.N.R. Rao, A crystallographic investigation of semiconductor to metal transition in pure and V_2O_3 doped Ti_2O_3 ., Curr. Sci. 46(13), 1977.
21. N.F. Mott, 'Metal-Insulator Transitions, Taylor and Francis, London, 1974.
22. C.N.R. Rao and G.V. Subba Rao, 'Transition Metal Oxides, NSRDS-NBS, Monograph 49, National Bureau of Standards, Washington, D.C., 1974.
23. L.L. Van Zandt, J.M. Honig and J.B. Goodenough, J. Appl. Phys., 39, 594, 1968.
24. G.V. Chandrashekar, Q.W. Choi, J. Moyo and J.M. Honig, Mat. Res. Bull., 5, 999, 1970.
25. R.E. Loehman, C.N.R. Rao and J.M. Honig, J. Phy. Chem., 73, 1781, 1969.
26. W.R. Robinson, J. Solid State Chem., 9, 255, 1974.
27. C.N.R. Rao, R.E. Loehman and J.M. Honig, Phys. Letts., 27A, 271, 1968.
28. B. Viswanathan, S. Usha Devi and C.N. Rao, Pramana, 1, 48, 1973.
29. R.E. Newnham and Y.M. de Hann, Z. Krist, 117, 235, 1962.
30. J.B. Goodenough, proceedings of the 10th International Conference on the Physics of Semiconductors, Cambridge, Mass. U.S.A., p. 304, 1970
31. S. Vasudevan, A.M. Shaikh and C.N.R. Rao, Jahn Teller effect induced phase transition in CsCuCl_3 , Phys. Lett. 70a, No. 1, 44, 1979.
32. A.W. Schlutetex, R.A. Jacobson and R.E. Rundle, Inorg. chem. 5(1966) 277.
33. C.J. Kroese, J.C.M. Tyndemans Van Eyndenhoven and W.J.A. Maskant, Solid State Commun., 9, 1707, 1971
34. S. Hirotsu, J. Phys. C10 (1977) 967.
35. G.A. Gehring and K.A. Gehring, Rep. Prog. Phys. 38 (1975) 1.
36. J. Fernandez, M.J. Teflo, J. Peraza and E.H. Bocanegra, Mat. Res. Bull. 11 (1976) 1161.
37. A.M. Shaikh and Subrata Ghose, 'Crystal structure of Zektzerite $\text{NaLiZrSi}_6\text{O}_{15}$ at 300, 773, 973, 1223 and 1323 K, NSF project (EAR 8206526) 'solid state chemistry', University of Washington Seattle, 1984.
38. A.M. Shaikh and Subrata Ghose, X-ray thermal expansion and phase transition study in Zektzerite $\text{NaLiZrSi}_6\text{O}_{15}$, NSF project (EAR 8206526) 'solid state chemistry' University of Washington Seattle, 1984.
39. A.M. Shaikh and Subrata Ghosh, A Second Order Phase Transition Induced by Na^+ -ion Order-Disorder in Zektzerite, $\text{NaLiZrSi}_6\text{O}_{15}$, Solid State Physics (India) Vol. 50, 141, 2005.
40. Ghose S. and Wan C. (1978) Zektzerite, $\text{NaLiZrSi}_6\text{O}_{15}$: a silicate with six-tetrahedral-repeat double chains. Am. Mineral., 63, 304–310.
41. J. Vicat and T Qui, 1982, unpublished results.
42. Duba A. G. and Ghose S. (1983) Electrical Conductivity and Ionic conduction mechanism in $\text{NaLiZrSi}_6\text{O}_{15}$ single crystals, Solid State Ionics, 9 & 10, 813–816.



A.M. Shaikh received the Ph.D. degree in Physics from Indian Institute of Science, Bangalore. He worked under the guidance of late Prof. M.A. Viswamitra in the field of high temperature Crystallography: Instrumentation and Phase transition X-ray during 1972–1977. In January, 1978 he joined the faculty of I.I.Sc. Bangalore as officer-in-Charge of CAD-4 X-ray diffractometer facility at Central Instruments and Services Laboratory. As a post doctoral research associate at University of Washington, Seattle U.S.A. during 1983–1984 he worked on high temperature crystal structure analysis of silicate minerals. In 1984 he joined University of Kuwait as Asst. professor of Crystallography and Mineralogy in Department of geological sciences. He worked on crystal chemistry of carbonate minerals, especially on Ikaite and Vaterite. In 1992 he joined Solid State Physics Division at Bhabha Atomic Research Centre, Mumbai and presently he is Scientific Officer (G), incharge of Neutron Detection and Neutron Radiography Laboratory. His current research interests are neutron & X-ray detectors, neutron radiography and hydrogen detection, neutron irradiation, neutron scattering and X-ray crystallography. He is associated with International Atomic Energy Agency programmes related to Neutron Radiography and worked as IAEA expert in this field. He has about 100 research papers in national and international journals and conference proceedings to his credit. Dr. Shaikh is on Board of Studies and Board of Ph.D. Examiners of many universities and research institutions in India. He is member of executive committee of Neutron Radiography Working Group, India (NRWG-I), Life member of Indian Crystallography Association, Indian Physics Association. He is recipient of DAE Technical Excellence Award 2004 and Indian Society for Nondestructive Testing (ISNT)-Nation Award-2003.